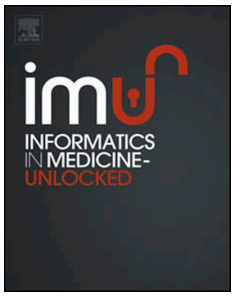

Are interconnected compartmental models more effective at predicting decompression sickness risk?

Gianluca Di Muro, F. Gregory Murphy, Richard D. Vann, Laurens E. Howle

PII: S2352-9148(19)30387-9

DOI: https://doi.org/10.1016/j.imu.2020.100334

Reference: IMU 100334

To appear in: *Informatics in Medicine Unlocked*

Received Date: 4 January 2020

Revised Date: 14 April 2020

Accepted Date: 23 April 2020

Please cite this article as: Di Muro G, Murphy FG, Vann RD, Howle LE, Are interconnected compartmental models more effective at predicting decompression sickness risk?, *Informatics in Medicine Unlocked* (2020), doi: https://doi.org/10.1016/j.imu.2020.100334.

Are Interconnected Compartmental Models More Effective at Predicting Decompression Sickness Risk?

Gianluca Di Muro[1], F. Gregory Murphy[1,2], Richard D. Vann[1,3], Laurens E. Howle[1,4,5,6]

[1] Department of Mechanical Engineering and Materials Science
Duke University
Durham, NC USA

[2]Navy Experimental Diving Unit
Panama City, FL

[3]Divers Alert Network
Durham, NC USA

[4]Department of Radiology
Duke University Medical Center
Durham, NC USA

[5]Division of Marine Science & Conservation
Duke University Marine Laboratory
Beaufort, NC, USA

[6]BelleQuant Engineering, PLLC
Mebane, NC USA

Tuesday, May 26, 2020

Corresponding author:
Laurens E. Howle, Ph.D., P.E., F.ASME
Department of Mechanical Engineering and Materials Science
Duke University
Durham, NC 27708-0300
919.660.5331 (office)
919.660.8963 (fax)
laurens.howle@duke.edu

ABSTRACT

Interconnected tissue compartmental models having two, three, or four compartments, one or more of which was risk-bearing, have been previously investigated for predicting the probability of decompression sickness (DCS) in compressed gas diving. We extend this prior work under general conditions to multiple risk-bearing compartments while providing exact risk function integrals. Four biophysical models based on different inter-compartmental connections ranging from uncoupled to fully coupled with bidirectional interaction were trained on a large data set to reject unjustified model parameters. We also explore how coupled models (and similar uncoupled models) perform for the prediction of DCS in humans when extrapolated to dives outside of the training set. The most successful model assumes slower tissues influence faster tissues with all compartments bearing risk and provide very good predictions for dives with surface decompression using oxygen.

KEYWORDS

Decompression sickness, optimization, diving, perfusion-diffusion models, multi-exponential exchange kinetics, probabilistic models, maximum likelihood.

INTRODUCTION

Decompression Sickness (DCS) is a condition which can occur in humans when there is a decrease of ambient pressure and can involve a variety of symptoms ranging from minor to fatal [1, 2]. Although it is generally accepted that DCS is initiated by the formation and growth of inert gas bubbles in the body [3], the mechanisms of its various forms are not completely understood. DCS can be encountered during diving, hyperbaric medical treatments, high altitude flights, and manned spaceflight operations [4]. Despite advances in methods for limiting the risk of DCS occurrence, it remains a significant challenge to operating in and exploring extreme environments.

Haldane *et al.* [5] are commonly credited as the first to provide an effective algorithm to significantly reduce DCS occurrences through a deterministic quasi-physiological mathematical model. He described the body as a parallel network of independent perfusion-limited tissue compartments in which the occurrence of DCS depended on the state of supersaturation in each of the tissues. They computed decompression schedules with this model which were more successful in comparison to previous methods at limiting DCS in compressed gas workers. In fact, in an experiment involving goats, they found that the proportion of illnesses with previous methodologies, based on uniform decompression schedules, was greater than with stage decompression though the stage decompression exposures completed the decompression in a third of the time. Yet, this approach was still not totally effective.

Noting the probabilistic nature of DCS in a rat model study by Berghage *et al.* [6], Weathersby [7, 8] introduced a probabilistic approach that treated DCS as a probabilistic binary variable where DCS = 1 if DCS occurred and DCS = 0 if DCS did not occur; although recent methods have been developed to simultaneously predict the probability and severity of

decompression sickness in humans [9]. This probabilistic approach had three modules: (a) a deterministic compartmental model, described by uncoupled Ordinary Differential Equations (ODEs) that computed the partial pressure of nitrogen in parallel tissue compartments; (b) a nonlinear function that mapped the instantaneous supersaturated nitrogen onto a probability that a diver would experience DCS; and (c) a body of empirical diving data that included depth-time dive profiles for many dives along with their binary DCS outcome. Modules (a) and (b) have undetermined parameters whose optimal values were found from the data in module (c) using the maximum likelihood approach which resulted in the best possible simulation of the empirical data by that model [10]. The likelihood approach has produced a large number of statistically-based decompression tables in which the DCS probability was controlled to target values over a wide range of dive exposures [11-26].

Notwithstanding the advances made during the last century in understanding fundamental DCS mechanisms and methods for computing decompression schedules, many uncertainties remain leading to a variety of alternative decompression procedures [27, 28] that still occasionally result in DCS [29]. Indeed, Doolette reported that Haldane's tables remain desirable in some cases [30]. The probabilistic models of DCS described above used parallel, perfusion-limited tissue compartments. The use of mono- or multi-exponential tissue kinetics was investigated in a dog model by Weathersby *et al.* [31, 32] using dilute ^{133}Xe breathed for a specified time interval. In fitting the radio-gas uptake and washout curves, the researchers found that at least two, frequently three, and occasionally four exponentials were needed to accurately fit the data. Novotny *et al.* [33] noted that a model based on parallel tissues failed to adequately describe experimentally measured ^{133}Xe washout from dog calf muscle. Doolette *et al.* [34-38] found that models including gas transport between tissue compartments were superior at

simulating experimental measurements of inert gas exchange in sheep brain and muscle when compared to models with uncoupled tissue compartments.

The first successful probabilistic decompression model for human divers was based upon a collection of uncoupled compartments [7, 11]. Later, models incorporating inter-tissue gas transport were derived from a deterministic model (the Kidd-Stubbs model) incorporating inter-tissue gas transport [39]. The Kidd-Stubbs model combined a series of four hypothetical tissues in series; with a single shared input/output to one of the distal compartments. Goldman [40] included inter-tissue gas transport in probabilistic decompression modeling in which he considered two or three inter-connected compartments with only the central compartment contributing to DCS risk and assumed linear dynamics in order to be able to integrate the equations analytically; yet, risk functions were estimated numerically. He suggested that this new class of models might potentially extrapolate better to dives not included in his truncated calibration data than the traditional parallel tissue models without inter-tissue perfusion.

In our previous works [41, 42], we extensively explored inter-tissue gas transfer models and other model structures based upon experimental work in sheep for use in predicting the probability of DCS in humans. Models containing coupled, perfusion-limited compartments – but with a single input and output – outperformed the traditional parallel, three-compartment, perfusion-limited models only for single air bounce dives. Models containing coupling with perfusion as well as diffusion – again with a single input and output – outperformed the same traditional parallel, three-compartment, perfusion-limited models for repetitive and multilevel air dives, dives with oxygen decompression, as well as single air dives. These findings support our conclusion that a combination of different uncoupled multi-compartment and single-compartment structures are likely needed to best describe diverse data sets.

The object of this paper is a detailed investigation of inter-tissue perfusion to determine if there is merit to Goldman's claims. We extend Goldman's model beyond two or three compartments, reduce the computational cost by replacing numerical with analytical integration, evaluate several risk-bearing tissue compartments rather than only one, and calibrate our new models to a larger set of dive profile data. Using linear algebra [49], we provide a general solution applicable to interactions between any number of compartmental tissues with linear combinations of exponential kinetics while guaranteeing a tissue matrix that remains characterized by distinct negative eigenvalues. We provide a general closed-form integral of the risk function that allows for fast estimation of DCS risk for numerous profiles without large computational cost. Further, we consider the case of multiple compartmental contributions to DCS risk; each having a different gain and a different risk threshold to account for differences between tissues. We explore the prediction capabilities, model failures, and model robustness when large data sets are used. We provide an efficient numerical algorithm to iterate through tissue matrices characterized by distinct real negative eigenvalues and propose a numeric methodology to restrict analysis to symmetric tissue matrices that may suggest physiological properties. Finally, we investigate the extrapolation of inter-tissue perfusion models in comparison to the well-known parallel tissue model EE1 [50, 51].

MATERIALS AND METHODS

Derivation of Inter-Connected Tissue Kinetics

Let the tissue partial tension vector, $\mathbf{p} \in \mathbb{R}^n$, be described by the following system of linear ordinary differential equations

$$\frac{d\mathbf{p}}{dt} = \mathbf{A}\mathbf{p} + \mathbf{f} \cdot p_{a,n}(t) \tag{1}$$

where we define $\mathbf{A} \in \mathbb{R}^{n \times n}$ the *tissue matrix* that is assumed to have distinct negative real eigenvalues; n is the number of well-stirred tissues, $\mathbf{f} \in \mathbb{R}^{n}$ is a vector, constant with respect to time, and $p_{a,n}(t)$ is the time varying arterial nitrogen partial pressure.

In agreement with Thalmann *et al.* [52] and Goldman [40], $p_{a,n}$ is assumed to be equal to the alveolar nitrogen partial pressure. Therefore, we can distinguish two cases, depending on the breathing gas conditions

$$p_{a,n}(t) = \left(1 - FI_{o_2}\right) \cdot \left[\, p^{a}(t) - p_{H_2O} \,\right] \tag{2}$$

for constant inspired fraction and

$$p_{a,n}(t) = p^{a}(t) - p_{H_2O} - PI_{O_2}(t) \tag{3}$$

for constant inspired partial pressure, as reported in equations (A13) and (A14) in appendix A of Goldman [40]; where $p^{a}(t)$ refers to the ambient hydrostatic pressure, p_{H_2O} to the water vapor partial pressure at body temperature (i.e., $37\,^{\circ}\mathrm{C}$), and finally FI_{o_2} and PI_{O_2} are the fraction of oxygen in the inspired gas and its partial pressure, respectively.

Throughout this derivation, we make the assumption of piecewise dive segments; thus, we can write $p^{a}(t)$ as an explicit function of time, so that

$$p^{a}(t) = p_0^{a} + r^{a} t \tag{4}$$

where p_0^{a} is the ambient hydrostatic pressure at time zero, and r^{a} is its rate of change with respect to time t. Similarly, we have an expression for the alveolar nitrogen partial pressure. In particular, it follows that $p_{a,n}(t)$ may be expressed as

$$p_{a,n}(t) = p_{a,n}(0) + r_{a,n} \cdot t \tag{5}$$

where the expression of the constants $p_{a,n}(0)$ and $r_{a,n}$ may be easily obtained, using Eq. (2) or Eq. (3). For example, in the case of constant inspired partial pressure, we get $p_{a,n}(0) = \left(1 - FI_{O_2}\right)\left(p_0^a - p_{H_2O}\right)$, and $r_{a,n}(t) = r^a\left(1 - FI_{O_2}\right)$. We impose the associated initial conditions, expressed as $\mathbf{p}_0 = \mathbf{p}(0) \in \mathbb{R}^n$ as the initial tissue nitrogen tension.

Let $\mathbf{A} = \mathbf{SDS}^{-1}$ be the spectral decomposition of the $\mathbf{A}$ matrix, so that $\mathbf{S}$ is the matrix of eigenvectors of $\mathbf{A}$, $\mathbf{D}$ is the diagonal matrix formed with the eigenvalues of , and let pose $\mathbf{p} = \mathbf{S}\boldsymbol{\varphi}$. Substituting into Eq. (1) we have the following system of uncoupled differential equations for $\boldsymbol{\varphi}$:

$$\frac{d\boldsymbol{\varphi}}{dt} = \mathbf{D}\boldsymbol{\varphi} + \mathbf{k}_1 + \mathbf{k}_2 \cdot t \tag{6}$$

where $\mathbf{k}_1 = \mathbf{S}^{-1}\,\mathbf{f}\; p_{a,n}(0)$, and $\mathbf{k}_2 = \mathbf{S}^{-1}\,\mathbf{f}\; r_{a,n}$, with the associated initial conditions $\boldsymbol{\varphi}_0 = \mathbf{S}^{-1}\mathbf{p}_0$. After some manipulations, we can write the general solution for $\mathbf{p}(t)$, as :

$$\mathbf{p}(t) = \mathbf{E}\boldsymbol{\mu}(t) + \boldsymbol{\xi} + \boldsymbol{\tau} \cdot t, \tag{7}$$

where $\mathbf{E} = \mathbf{SC}$, with $\mathbf{C} = \sum_{i=1}^{n} c_i \mathbf{e}_i \otimes \mathbf{e}_i$, having addressed with $\otimes$ the tensor product applied to vectors, $\mu_i(t) = e^{\lambda_i t}$, $i = 1, 2, \ldots, n$, $\boldsymbol{\xi} = \mathbf{S}\boldsymbol{\delta}$, $\boldsymbol{\tau} = \mathbf{S}\boldsymbol{\varepsilon}$ with $\delta_i = -\frac{k_{2i}}{\lambda_i^2} - \frac{k_{1i}}{\lambda_i}$, $\varepsilon_i = -\frac{k_{2i}}{\lambda_i}$, and with λ_i the i-th eigenvalue of $\mathbf{A}$, assumed to be distinct and strictly negative to ensure stability.

Analytical Integration of the Risk Function

As proposed in Goldman [40], adopting the formulation proposed by Thalmann *et al.* [52], we can write the i-th component of the risk function, $\boldsymbol{\rho}$, as

$$\rho_i = \frac{p_i(t) - \left[p^a(t) + b_i \right]}{p^a(t)} \tag{8}$$

where b_i is constant with respect to time and represents the pressure threshold of the *i*-th tissue compartment and $p_i(t)$ is its tissue partial tension, provided by (7)**Error! Reference source not found.**. Eq. (8) simply states that in each kinetic compartment the risk is proportional to the relative supersaturation above a certain threshold b_i. We are aiming to evaluate the hazard vector $\boldsymbol{\zeta}$, defined as $\boldsymbol{\zeta} = \int_{t_i}^{t_f} \boldsymbol{\rho}\, dt$, since the probability of developing DCS is related to this function through the following expression

$$P_{DCS} = 1 - e^{-\boldsymbol{\alpha}\cdot\boldsymbol{\zeta}} \tag{9}$$

where t_i and t_f are the initial and the final times of the dive segment, respectively, with $\boldsymbol{\alpha} \in \mathbb{R}^n$ a vector of tissue compartment gains that is assumed to be constant with respect to time. While Goldman [40] assumes that only the first compartment contributes directly to DCS risk, we choose to keep a general notation in our derivation. Specifically, Goldman's models are found by imposing $\boldsymbol{\alpha}$ to be $[\alpha \quad 0 \quad 0]^T$ and $[\alpha \quad 0]^T$ for his three (3CG and 3CM) and two compartment models (2CG and 2CM), respectively.

We integrate the function starting from a general initial time and break the integral into parts where the risk function becomes negative. To evaluate the integral, it is more convenient to rewrite the expression for $\boldsymbol{\rho}$ in terms of linear operators so that they may be removed from the integration. After substituting Eq. (7)**Error! Reference source not found.** into Eq. (8) and simplifying, we have the following expression for $\boldsymbol{\rho}$

$$\boldsymbol{\rho}(t) = \mathbf{E}\mathbf{v}(t) + \bar{\boldsymbol{\xi}}\, y(t) + \boldsymbol{\tau}\, \omega(t) - \mathbf{u}. \tag{10}$$

where the following definitions apply in Eq. (10)

$$\mathbf{v}(t) = \left[\frac{e^{\lambda_1 t}}{p^a(t)} \quad \frac{e^{\lambda_2 t}}{p^a(t)} \quad \cdots \quad \frac{e^{\lambda_n t}}{p^a(t)} \right]^T, \tag{11}$$

$$\overline{\boldsymbol{\xi}} = \boldsymbol{\xi} - \mathbf{b} \tag{12}$$

$\mathbf{y}(t) = \dfrac{1}{p^a(t)}$, $\boldsymbol{\omega}(t) = \dfrac{t}{p^a(t)}$, and finally

$$\mathbf{u} = \overbrace{\left[1 \quad 1 \quad \cdots \quad 1 \right]^T}^{n}. \tag{13}$$

With these assumptions, we can estimate $\boldsymbol{\zeta}$, as

$$\boldsymbol{\zeta} = \mathbf{E}\int_{t_i}^{t_f} \mathbf{v}(t)\, dt + \overline{\boldsymbol{\xi}}\int_{t_i}^{t_f} y(t)\, dt + \boldsymbol{\tau}\int_{t_i}^{t_f} \omega(t)\, dt - (t_f - t_i)\mathbf{u}. \tag{14}$$

Every term on the right-hand-side of Eq. (14) must be evaluated. With the assumption of piecewise dive segments, we can impose Eq. (4), the definition of the ambient hydrostatic pressure. Then, we must distinguish two cases for each term: when $r^a \neq 0$ and when $r^a = 0$. After some manipulation, we get the following expressions:

$$\int_{t_i}^{t_f} \nu_i(t)\, dt = \int_{t_i}^{t_f} \frac{e^{\lambda_i t}}{p_0^a + r^a t} dt = -\frac{1}{r^a} e^{-\overline{\lambda}_i} \left[EI\left(\overline{\lambda}_i + \lambda_i t_f\right) - EI\left(\overline{\lambda}_i + \lambda_i t_i\right) \right], \text{ for } r^a \neq 0 \tag{15}$$

and

$$\int_{t_i}^{t_f} \nu_i(t)\, dt = \int_{t_i}^{t_f} \frac{e^{\lambda_i t}}{p_0^a} dt = \frac{1}{p_0^a \lambda_i} \left(e^{\lambda_i t_f} - e^{\lambda_i t_i} \right), \text{ for } r^a = 0 \tag{16}$$

where we have introduced the modified eigenvalue $\overline{\lambda}_i$, defined as : $\overline{\lambda}_i = \lambda_i \frac{p_0^a}{r^a}$, for $i = 1, 2, \ldots, n$.

In Eq. (15), $EI(t)$ refers to the exponential integral function, as defined in Abramowitz and Stegun [53], that is, $EI(t) = \int_{-\infty}^{t} \frac{e^x}{x}\, dx$. Similarly, for the other scalar terms, we have

$$\int_{t_i}^{t_f} y(t)\, dt = \int_{t_i}^{t_f} \frac{dt}{p_0^a + r^a t} = \frac{1}{r^a} \ln\left(\frac{p_0^a + r^a t_f}{p_0^a + r^a t_i} \right), \text{ for } r^a \neq 0 \tag{17}$$

and

$$\int_{t_i}^{t_f} y_i(t)\, dt = \int_{t_i}^{t_f} \frac{dt}{p_0^a} = \frac{t_f - t_i}{p_0^a}, \text{ for } r^a = 0. \tag{18}$$

Finally, for the integral of $\omega(t)$ to be evaluated in Eq. (14), we have

$$\int_{t_i}^{t_f} \omega_i(t)\, dt = \int_{t_i}^{t_f} \frac{t}{p_0^a + r^a t}\, dt = \frac{t_f - t_i}{r^a} + \frac{p_0^a}{\left(r^a\right)^2} \ln\left(\frac{p_0^a + r^a t_i}{p_0^a + r^a t_f} \right), \text{ for } r^a \neq 0 \tag{19}$$

and

$$\int_{t_i}^{t_f} \omega_i(t)\, dt = \frac{1}{p_0^a} \int_{t_i}^{t_f} t\, dt = \frac{t_f^2 - t_i^2}{2 \cdot p_0^a}, \text{ for } r^a = 0. \tag{20}$$

Equations (15)-(20) are the relations needed to evaluate Eq. (14) and, therefore, the DCS probability by using Eq. (9).

Integration of Positive Definite Portion of the Risk Function

When estimating the probability of DCS, we have to neglect any interval where the risk function attains negative values. To achieve this, we must find the risk function roots and check for sign changes. Since the risk function is continuous on its interval of definition, Bolzano's theorem [54] applies.

Recalling Eq. (8), we have to study the sign of the following function

$$\text{sign}\left[\rho_k(t)\right] = \text{sign}\left\{p_k(t) - \left[p^a(t) + b_k\right]\right\}, \quad \text{for } k = 1, 2, \ldots, n. \tag{21}$$

Making use of the general solution for the compartment tissue pressure, the generic component of the risk function vanishes at time $\bar{t}$, if and only if

$$\bar{t} \Big| \sum_{j=1}^{n} E_{ij} e^{\lambda_j \bar{t}} + \xi_i + \tau_i \cdot \bar{t} = \left(p_0^a + r_a \cdot \bar{t} + b\right). \tag{22}$$

The last expression is non-linear with respect to the scalar unknown $\bar{t}$, but decoupled, so without loss of generality, the generic scalar equation can be solved. Rearranging similar time-dependent terms, we can rewrite Eq. (22), as

$$t^0 \Big| \sum_{j=1}^{n} E_j e^{\lambda_j t^0} - \chi \cdot t^0 - \eta = 0 \tag{23}$$

where we have defined the following quantities

$$\chi = \left(r_a - \tau\right) \tag{24}$$

and

$$\eta = \left(p_0^a + b - \xi\right). \tag{25}$$

To find the roots of Eq. (23), if any, we proceed as follows. First, each integration interval was subdivided into S sub-intervals of equal length. Then, with t_i^j and t_f^j as the initial and final times of the *j*-th sub-interval, respectively, we evaluate $h_j = \rho\left(t_i^j\right) \cdot \rho\left(t_f^j\right)$, for $j = 1, 2, \ldots, S$. For every sub-interval for which we found $h_j < 0$, we applied the Dekker-Brent method [55], to find the internal root. We choose this algorithm for its robustness and fast convergence and check the sign of the risk between successive roots, including the two most external intervals starting from

t_i and arriving to t_f. We labeled intervals where the risk function attained negative values and excluded these from the integration.

Selection of Model Parameters

The analytical derivation presented so far is completely general and applicable to all models governed by linear coupled ordinary differential equations. However, to assess the goodness-of-fit for a specific model to calibration data, some assumptions have to be made on the form of the matrix $\mathbf{A}$, the vector $\mathbf{f}$, and their dimensions. How many tissue compartments to consider, for example, which parameters to vary, and which constraints to apply are not trivial choices. Choosing too few parameters might result in a sub-optimal fit of the calibration data whereas choosing too many might over-fit the data leading to poor extrapolation to dives not in the calibration data. In this section, we review previous research and in the next section, derive a new class of models. This will allow a contrast between previous and newer work.

Goldman [40] presents four new multi-exponential models: two couples of two (2CG and 2CM) and three compartments (3CG and 3CM), respectively, in which only one compartment is assumed to directly contribute to DCS risk. This risk-bearing compartment is associated with the eigenvalue having the largest absolute value. The Goldman models define the maximum number of free parameters within the tissue matrix $\mathbf{A}$ as the number of tissues, n, or the number of distinct eigenvalues. For 3CG, 3CM and 2CG, 2CM, this requires only three and two parameters, respectively. We argue, however, that all free parameters of the model (not just the number of tissues) must be evaluated, and a given parameter rejected only if it fails a likelihood ratio test.

Inspecting Goldman's three tissue compartment models, the $\mathbf{A}$ matrix has the form

$$\mathbf{A}=\begin{pmatrix} -3f_{1x} & f_{1x} & f_{1x} \\ f_{21} & -(1+\mathrm{PR}_2)\,f_{21} & 0 \\ f_{31} & 0 & -(1+\mathrm{PR}_3)\,f_{31} \end{pmatrix};\quad \mathbf{f}=\begin{pmatrix} f_{1x} \\ \mathrm{PR}_2\ f_{21} \\ \mathrm{PR}_3\ f_{31} \end{pmatrix} \tag{26}$$

where the following additional constraints were imposed to evaluate Eq. (26): $\mathrm{PR}_2=\mathrm{PR}_3=0.2$ and $\mathrm{PR}_2=\mathrm{PR}_3=0$ for the 3CG and 3CM, respectively. They represent the "perfusion ratio", defined as "diffusion rate constants" out of the generic compartment "*i*". They were set arbitrarily to 0.2, to illustrate the properties of the models; whereas they vanish, in the case of a mammillary model, since the connections of compartments 2 and 3 with the circulatory system are severed by assumption. This construction guarantees negative and generally distinct eigenvalues if the free parameters are strictly positive, but these constraints are arbitrary and only used for testing. The connections between the second and the third compartments were also severed. The two compartment tissue models are obtained from the previous models by reducing the degrees of freedom to two and considering a two-by-two system similar to the three-tissue case.

Algorithm for Iterating through Stable Matrices and Choice of Forcing Term

In this section, we remove all or most of the assumptions of Goldman [40] and select models based on the form of the $\mathbf{A}$ matrix as before while only considering cases associated with strictly negative distinct eigenvalues. We formulate our assumptions starting from the matrix spectral decomposition to clarify how the forcing term may be conveniently related to the tissue matrix.

Recall our matrix spectral decomposition

$$\mathbf{A}=\mathbf{S}\mathbf{D}\mathbf{S}^{-1}. \tag{27}$$

By selecting models based on the properties of $\mathbf{S}$ and $\mathbf{D}$, we can easily impose any spectral property of $\mathbf{A}$ and use Eq. (27) to derive $\mathbf{A}$ *a posteriori*. To consider only negative and distinct

295 eigenvalues, we trivially impose $\mathbf{D} = \mathrm{diag}(\lambda_1, \lambda_2, \ldots, \lambda_n)$, choosing $0 > \lambda_n > \lambda_{n-1} > \ldots > \lambda_1$,
296 without loss of generality and maintaining Goldman's convention of choosing the first
297 compartment as that associated with the smallest eigenvalue. In so doing, we start from the
298 tissue times, as is done with independent tissue models in a more physiological manner.

299 Any invertible diagonalizable matrix, $\mathbf{S}$, is appropriate but may have redundant
300 parameters since the eigenvector matrix is not unique. We restrict our choice of free parameters
301 by considering independent tissue compartments that may be obtained as a limiting case from
302 our general formulation by imposing, e.g., $\mathbf{S} = \mathbf{I}$, where $\mathbf{I} \in \mathbb{R}^{n \times n}$ is the identity matrix. This
303 observation suggests that we can relate the difference between the eigenvector matrix $\mathbf{S}$ and the
304 identity matrix to the degree of dependency among the different compartments. Without loss of
305 generality, we impose equality among the elements of the main diagonal of $\mathbf{S}$ since they are
306 arbitrary multipliers of the eigenvalues in $\mathbf{A}$ and assume they are equal to one. It is trivial to
307 prove a matrix $\mathbf{A}$ may be spectrally decomposed by Eq. (27), through an eigenvector matrix $\mathbf{S}$,
308 whose main diagonal elements are one under the assumption of distinct eigenvalues. With this
309 choice for $\mathbf{S}$, we have n^2 free parameters, $n(n-1)$ for the generic choice of components of $\mathbf{S}$
310 outside the main diagonal plus *n* eigenvalues that we would have by considering $\mathbf{A}$.

311 We constrain the forcing term multipliers addressed by the vector $\mathbf{f}$ through the choice of
312 the matrices $\mathbf{S}$ and $\mathbf{D}$ by inspecting a steady-state solution. Specifically, our model produces a
313 constant tissue pressure if we assume a dive profile characterized by constant arterial nitrogen
314 tension with the initial condition that all tissue tensions are approximately equal to this constant
315 value. For this special case, all derivatives of the partial tissue tension with respect to time must
316 vanish. Hence,

317 $$\mathbf{0} = \mathbf{A}\mathbf{p} + \mathbf{f}\, p_{a,n}. \tag{28}$$

With the hypothesis that $\mathbf{p} = p_{a,n}\mathbf{u}$, where $\mathbf{u}$ is the constant unit vector defined in Eq. (13), we have the following required expression for the forcing term

$$\mathbf{f} = -\mathbf{A}\mathbf{u}. \tag{29}$$

Equation (29) is consistent with both independent and uncoupled tissues as in the Goldman models.

Algorithm for Iterating through Symmetric Matrices

We begin by investigating a balanced nitrogen contribution between any two tissue compartments, i.e., symmetric tissue matrices in which the contribution to the *j*-th tissue provided by the *i*-th tissue is equal to that exerted by the *j*-th tissue to the *i*-th tissue. This requires iteration through symmetric matrices starting from their spectral decomposition for which we propose a simple algorithm.

Recalling Eq. (27), we constrain $\mathbf{S}$ so that $\mathbf{A}$ is a symmetric matrix where $\mathbf{S}$ is orthogonal since a real matrix is symmetric if and only if it has an orthonormal basis of eigenvectors [52]. Thus, we have

$$\mathbf{A} = \mathbf{S}\mathbf{D}\mathbf{S}^{-1} = \mathbf{S}\mathbf{D}\mathbf{S}^{T}. \tag{30}$$

Let $\bar{\mathbf{u}}_i, i = 1,2,\ldots,n$, be the generic column vectors of $\mathbf{S}$ which are eigenvectors of $\mathbf{A}$. First, we arbitrarily choose $n-1$ components, $\hat{r}_i = \left[\varpi_i^1 \varpi_i^2 \cdots \varpi_i^{n-1}\right], i = 1,2,\ldots,n$, for each column of $\mathbf{S}$. Then, we rescale for a known scalar greater than their Euclidean norm, so that $\mathbf{r}_i = \dfrac{\hat{\mathbf{r}}_i}{\bar{K}\left\|\hat{\mathbf{r}}\right\|_2}, i = 1,2,\ldots,n$, with $\bar{K} > 1$. If, for example, we suppose that $\bar{K} = 1.1$, we compute the last components $\left\|\mathbf{u}_i\right\|_2 = 1, i = 1,2,\ldots,n$. We apply the modified Gram-Schmidt process [49] and derive the *n*-th column of the orthogonal $\mathbf{S}$ matrix making $\mathbf{A}$ symmetric.

Model Calibration: Maximum Likelihood Estimation

Maximum likelihood is a statistical method used for comparing the relative goodness of fit of models to given calibration data [7, 56, 57]. We review this method below to show how it relates to DCS probabilities estimated in the previous sections.

Equation (9) expresses the probability that a diver experiences DCS. The probability of not experiencing DCS plus the probability of experiencing DCS must equal one by the law of total probability implying that

$$P_0 = e^{-\boldsymbol{\alpha}\cdot\boldsymbol{\zeta}}. \tag{31}$$

Suppose that our calibration data consist of D dives with known outcomes. The likelihood function of the entire data set is the joint probability of observing the entire trial,

$$\mathrm{L}(\text{trial}) = P(\text{obs } 1)\,P(\text{obs } 2)\cdots P(\text{obs } D), \tag{32}$$

as reported in [7]. The probability of observing the *j*-th event with $j = 1,\ldots,D$ is

$$P(\text{obs } j) = P_{DCS}(\text{dive } j)^{\delta_j}\, P_o(\text{dive } j)^{1-\delta_j} \quad j = 1,2,\ldots,D, \tag{33}$$

where δ_j is the outcome variable and equal to one for full DCS and zero for no DCS. A marginal DCS event was weighted as 0.1 full DCS event for comparison with Goldman's results [40] although Howle *et al.* [58] argued that marginal events should not be used for DCS parameter calibration; an assertion that was later investigated by Murphy *et al.* [59] for generating iso-risk air diving schedules, where several optimal ascent schedules have been obtained, for a given tolerated risk of developing DCS.

The natural logarithm of the likelihood is used to avoid extremely low values as this monotonic transformation preserves the order of the function [7]. Therefore, the natural log likelihood (LL) of the calibration data is estimated with the following expression:

$$\mathrm{LL}(\text{trial}) = \sum_{j=1}^{D} \log\left[P(\text{obs } j)\right]. \quad (34)$$

Although not explicitly expressed in Eq. (34), the LL value depends on the model parameters through probability estimates and observed outcomes. To find the parameter values that maximize Eq.(34), we have to solve an optimization problem. We note that Eq. (34) generally constitutes a nonlinear non-convex optimization, making it difficult to solve with local optimization methods, based on the gradient descent, because they can be trapped in local minima [60, 61]; thus we adopted the Nelder-Mead algorithm [62] chosen for its robustness and ability to handle ill-conditioned problems. It is worth noting that, as an alternative to log likelihood maximization, Bayesian methods have recently been shown to be beneficial in optimizing probabilistic decompression sickness models [63].

RESULTS AND DISCUSSION

Having derived general solutions to the interconnected tissue model, we now apply these solutions with a large calibration data set known as "BIG292" [64]. Our objective is to evaluate how the sub-set of the general model derived by Goldman [40] will extrapolate to this larger dataset and to compare these results with the performance of the general model. First, we describe the data and then fit Goldman's most general model (3CG) to this data set. Next, we describe four novel interconnected models and fit these to BIG292. Last, we compare all models with the equivalent independent tissue model (EE1 [50, 51]) to verify whether the extra parameters of the new models are justifiable by the likelihood ratio test. Finally, we examine how well all models extrapolate (predict the observed outcomes) of data not included in the BIG292 calibration data.

382 The conditions through which the dives are conducted may greatly impact, among other
383 factors, the rate of blood circulation, which -in turn- affect the amount of excess nitrogen given
384 off through the lungs [5], thus ultimately influencing the likelihood of being affected by DCS.
385 Therefore, it is pivotal to rely on high quality data, reporting the circumstances under which
386 dives occurred, to have a proper calibration of DCS models. Moreover, it is crucial to have a
387 consistent definition of DCS events, throughout the study. For collecting the data constituting
388 the BIG292, Weathersby *et al* "developed a set of diagnostic criteria […] to serve as a
389 retrospective tool in determining what symptoms and signs were to be regarded as DCS".
390 Furthermore, the conditions under which the dives occurred are clearly identified; for example:
391 dry dives, where variation between subjects is minimal and the time-depth profile is finely
392 controlled versus wet dive where a less controlled environment is present and exercise and
393 thermal factors influence represent nuisance variables.

394 The U.S. Navy has used BIG292 extensively for calibrating probabilistic decompression
395 models. It consists of 3,322 Air and Oxygen-Nitrogen exposures resulting in 190 full DCS and
396 110 marginal DCS cases. The BIG292 dive data, together with thousands of additional dive
397 trials are publicly available in two U.S. Government reports [64, 65]. Because these data are
398 randomized, de-identified, and publicly available, no IRB approval was required for this study.
399 The data were collected by the U.S., U.K. and Canadian military facilities from 1944 to 1997 and
400 include detailed time-depth histories, inspired gas(es), gas switches, and case reports for divers
401 with full or marginal DCS. To be consistent with Goldman's approach, we weighted marginal
402 DCS as 0.1 but did not consider symptom onset times [8]. Conversely, the risk thresholds, vector
403 **b** in Eq. (8), was not set *a priori* and was included in the models to be optimized, whereas
404 Goldman fixed it to 0.021 [40].

When we evaluated the 3CG model on BIG292 using the published optimal parameter set, it predicted zero DCS probability on 73 dive profiles where DCS does occur. This is described as *model failure*. We attempted to re-optimize this model using the aforementioned parameter set as the starting point for the optimization but were unsuccessful again. Finally, we sampled the likelihood function and adopted more than 110,000 random starting points chosen from a pseudo random uniform distribution around the optimal set with a range of 1/4 to 4 times the optimal parameter values. Again, this resulted in model failure leading us to conclude that the 3CG model will not fit the BIG292 data set without model modification.

Next, we evaluated four novel interconnected models based on the spectral decomposition described in the previous section. The models differed depending on assumptions pertaining to the eigenvector matrix **S**. We examined three tissue models that differed from Goldman in that all compartments were DCS-risk-active.

The following forms for the eigenvector matrix were considered: 1) Upper Triangular (UT); 2) SKew-symmetric (SK); 3) SYmmetric (SY); 4) GeNeral (GN). UT also produces an upper triangular tissue matrix: since, if **S** is upper triangular, then **A** will necessarily also be so. This will make interpretation of the physical elements more direct, because the eigenvalues of an upper triangular matrix can be promptly read on the matrix main diagonal. Also, since the tissues are ordered according to increasing eigenvalues, this model assumes that the contribution of faster tissues to slower tissues may be neglected in estimating the DCS risk: because, for definition of an upper triangular matrix, we have that $a_{ij} = 0$ if $i > j$. SK and SY were adopted to investigate whether algebraic constraints on the eigenvector matrix may be compatible with the data or may have better extrapolation properties. The skew-symmetric matrix refers exclusively to the components off the main diagonal since the main diagonal of a complete

skew-symmetric matrix would be all zeros resulting in a singular matrix. Finally, the GN model was the most general model and investigated whether all extra parameters were justifiable or were useful for extrapolation to data not in the calibration data set.

Figure 1 sketches the differences among the EE1, Goldman's 3CG and the most general model introduced in this paper (GN). In the EE1 model and in the models proposed here all tissue compartments contribute directly to DCS risk, whereas in Goldman's models only the central compartment, characterized by the smallest eigenvalue, has a nonzero risk gain. EE1 does not include any inter-perfusion phenomenon, while Goldman's models assume only inter-perfusion between an external compartment and the central compartment; our model generalizes it and includes connections between any two compartments.

For example, consider a simple derivation of the UT model with the optimal set reported in

Table **1**. For the eigenvector matrix, we have posed, $s_{ii}=1,\ i=1,2,\ldots,n$ without loss of generality, and for the specific model we have $s_{ij}=0,$ if $i>j, i=1,2,\ldots,n.$ Once we have evaluated **S**, we can compute $\mathbf{S}^{-1}$ and derive **A**, through Eq. (27). Finally, we evaluate the vector **f**, through Eq. (29). Since

$$\mathbf{S}=\begin{bmatrix}1 & -0.066 & 0.572\\ 0 & 1 & -2.899\\ 0 & 0 & 1\end{bmatrix},\ \text{we get: } \mathbf{A}=\begin{bmatrix}-0.917 & -0.060 & 0.348\\ 0 & -0.008 & -0.018\\ 0 & 0 & -0.002\end{bmatrix},\ \text{and } \mathbf{f}=\begin{bmatrix}0.629\\ 0.026\\ 0.002\end{bmatrix}.$$

The remaining free parameters are the optimal gains, which may be found analytically [66], and the thresholds as reported in

Table **1**.

450

Figure 2 schematizes the connections among the three tissues of the UT model. The radii of the circles reflect the value of the corresponding tissue eigenvalues. All relative terms were scaled for the absolute value of the corresponding eigenvalue for each tissue. Arrow thickness represents the strength of the interaction although the figure is not to scale. The direction of the arrows indicates the direction of the interaction for a positive increment of the relative variable. For example, the a_{23} term indicates the effect a change in the third tissue tension has on the rate of change in the second compartment. Since the arrow departs from the second tissue, we infer that a positive increment in p_3 contributes to a decrement on p_2. The double arrow (a_{23}) indicates a value roughly double its corresponding eigenvalue. The other models follow the same technique and are not discussed. We emphasize that any other coupled model may be expressed through our formulation under the assumptions of unique, negative eigenvalues, and a diagonalizable tissue matrix. We can compute **S** and **D**, for example, knowing **A** for Goldman's 3CG optimal model. The computed **S** will not always satisfy our assumption of the main diagonal occupied by ones, however, we can obtain an equivalent matrix from any representation of **S** by dividing each column by its diagonal term. Should we have a zero on the main diagonal, it suffices to change the numeration of the column of our problem since we can exclude a whole row of zeros because **S** is always non-singular.

For all models, we tried at least 128 random restarts to search for the best parameter set using parallel processing and did not consider onset times, as already stated. At first, we optimized the EE1 model, taken as a benchmark, comprised of three independent tissue compartments. EE1 has nine adjustable parameters: three tissue time constants, three tissue gains, and three pressure thresholds. Once we found the optimal parameter set for EE1, we used it as a starting point for all the interconnected models. This is possible because all models,

474 including EE1, are part of a nested set within the general model so its solutions exist within the
475 general solution space where the terms of the main diagonal of the eigenvector matrix are all
476 ones.

477 We adopted best optima from the UT, SK and SY models as starting optimization points
478 for the GN model. Optimal parameter sets with LL values are shown in

479

Table 1. Confidence intervals were computed by inverting the likelihood ratio test [67] using a Monte Carlo method and are reported as variations from the optimal value in superscript and subscript.

Table 2 contrasts the various models using a likelihood ratio (LR) test and indicates that the extra parameters for the coupled models are justified with a confidence of at least 95%. Nevertheless, the SY has a decrement of only 0.12 LL units compared with the GN model despite GN having three additional parameters, so GN does not pass the LR test when compared with the SY and UT models. However, GN is better than the SK and UT models. This suggests that SY is the preferred model when fit to BIG292. Table 3 provides a detailed description of the predicted DCS probabilities for all four coupled models and compares them with the EE1 model. All models fit the data with reasonable accuracy, based on risk prediction. The results suggest that the optimized SY outperforms EE1for all dive types except for saturation and multi-level dives.

To assess the extrapolation properties of the models, we considered 5,163 exposures comprised of Air and Oxygen-Nitrogen dives and surface O_2 decompression dives that resulted in 214 full DCS and 329 marginal DCS events. We extracted this data set, from the original data sets contained in [55-56] pulling all the data pertaining to the same dive profile, together. Table 4 compares the risk prediction of the four interconnected models with EE1. The UT model clearly out-performs all the other models both for LL and the number of predicted DCS cases. Table 4 also reports partial LL values grouped according to dive type in an effort to establish when coupled models may be worse than EE1 or if a particular model would seem to better extrapolate for a specific type of dive. The results indicate that SY (and GN, consequently) also outperforms EE1 and the abrupt decrement in the total LL is mainly due to poor performance for

submarine escape dives. On the contrary, UT is confirmed as the best coupled model considered in this work, and even if it also greatly overestimates the DCS risk for this kind of dive, it is still considerably better than any other model. Conversely, EE1 still remains the best model when evaluated on single air dives, both in terms of predicting risk and in terms of LL measure. Overall, the best coupled model, UT, presents a percentage error less than 5% when estimating the total number of DCS cases on the whole extrapolation set, as opposed to more than 24% when adopting the equivalent uncoupled model, EE1. Finally, we observe the superior predictions for the UT model on surface O_2 decompression and higher LL than other models of similar degrees-of-freedom.

CONCLUSION

We investigated the fitting quality and extrapolation capabilities of coupled compartmental models for predicting DCS probability in compressed gas diving. The motivation for this work was to investigate certain tissue compartment couplings with an *a-priori* specification of the coupling structure. Our coupled compartmental models allowed, in the most general case, for inert gas exchange with the circulatory system and between all individual compartments. We proposed a new formulation of the coupled tissues model based on the spectral decomposition of the tissue interconnection matrix and further derived piecewise exact gas exchange solutions for the new models. The exact solutions represent a projection of the original problem onto a space spanned by the eigenvectors of the tissue coupling matrix. In the space of the projected problem, the "compartments" decouple from one another making the problem far simpler and faster to optimize. Our interconnected models have, as a trivial subset, a well-tested parallel tissue model (EE1) allowing for rigorous comparison between our new models and this previous parallel model. Four distinct types of tissue interconnections were

526 considered and arose naturally from the form of the off-diagonal structure of the eigenvector
527 matrix. These four classes of interconnected models were the (1) skew-symmetric, (2) general,
528 (3) upper triangular, and (4) symmetric models. The symmetric interconnected model had the
529 best predictive quality for the training data set. In comparison to all four new interconnected
530 models, the nested parallel model (EE1) was rejected with at least 95% confidence. Although
531 the best of the inter-connected models to fit the calibration data was the symmetric model, the
532 upper triangular model extrapolated better to dive profiles outside of the training data set. The
533 upper triangular model also outperformed all of the other models on O_2 surface decompression
534 dive profiles. There are many extensions of our new models yet to be explored, for example, the
535 use of DCS symptom onset times in optimizing the models and gas saturation/bubble phase
536 change, as well as the introduction of some penalization to ensure a minimum good fit to each
537 subset of DCS for each diving type but the preliminary results presented in this paper indicate
538 that our new models are promising for use in predicting DCS probability and for dive planning.
539

540 **ACKNOWLEDGEMENTS**

541 We would like to thank Drs. Wayne Gerth and David Doolette, both of the Navy
542 Experimental Diving Unit, for their reviews of this paper and for their helpful comments. This
543 work was supported by Naval Sea Systems Command (NAVSEA-00C -
544 http://www.navsea.navy.mil/) under contracts #N61331-06-C-0014, #N00024-13-C-4104 and
545 #N00024-17-C-4317 and the Office of Naval Research under grant N000141310063. BelleQuant
546 Engineering, PLLC provided computational resources. Neither the funding agency nor the
547 commercial entity played any role in designing this study, data collection and analysis, decision
548 to publish, interpreting the results, or writing the manuscript.

REFERENCES

[1] R.D. Vann, F.K. Butler, S.J. Mitchell, R.E. Moon, Decompression illness, Lancet, 377 (2011) 153-164.

[2] R.D. Vann, D. P.J., L.E. Howle, P.W. Weber, J.J. Freiberger, C.F. Pieper, Resolution and severity in decompression illness, Aviation Space and Environmental Medicine, 80 (2009) 466-471.

[3] R.D. Vann, Mechanisms and Risks of Decompression, in: A.A. Bove, J.C. Davis (Eds.) Bove and Davis' diving medicine, Saunders, Philadelphia, 2004, pp. 127-164.

[4] R.E. Moon, R.D. Vann, P.B. Bennett, The physiology of decompression illness, Scientific American, 273 (1995) 59-61.

[5] A.E. Boycott, G.C.C. Damant, J.S. Haldane, The prevention of compressed air illness, Journal of Hygiene, 8 (1908) 342-443.

[6] T.E. Berghage, J.M. Woolley, L.J. Keating, The probabilistic nature of decompression sickness, Undersea Biomedical Research, 1 (1974) 189-196.

[7] P.K. Weathersby, L.D. Homer, E.T. Flynn, On the likelihood of decompression sickness, Journal of Applied Physiology, 57 (1984) 815-825.

[8] P.K. Weathersby, S.S. Survanshi, L.D. Homer, E. Parker, E.D. Thalmann, Predicting the time of occurrence of decompression sickness, Journal of Applied Physiology, 72 (1992) 1541-1548.

[9] L.E. Howle, P.W. Weber, E.A. Hada, R.D. Vann, P.J. Denoble, The probability and severity of decompression sickness,PLoS One 12(3), 2017.

[10] A.W.F. Edwards, Likelihood; an account of the statistical concept of likelihood and its application to scientific inference, University Press, Cambridge Eng., 1972.

[11] P.K. Weathersby, S.S. Survanshi, L.D. Homer, B.L. Hart, R.Y. Nishi, E.T. Flynn, M.E. Bradley, Statistically Based Decompression Tables I: Analysis of Standard Air Dives: 1950-1970., in: U.S. Navy (Ed.), 1985.

[12] P.K. Weathersby, J.R. Hays, S.S. Survanshi, L.D. Homer, B.L. Hart, E.T. Flynn, M.E. Bradley, Statistically Based Decompression Tables II: Equal Risk Air Diving Decompression Schedules, in: U.S. Navy (Ed.)Bethesda, MD, 1985.

[13] P.K. Weathersby, S.S. Survanshi, J.R. Hays, M.E. MacCallum, Statistically Based Decompression Tables III: Comparative Risk Using U.S. Navy, British, and Canadian Standard Air Schedules, in: U.S. Navy (Ed.)Bethesda, MD, 1986.

[14] J.R. Hays, B.L. Hart, P.K. Weathersby, S.S. Survanshi, L.D. Homer, E.T. Flynn, Statistically based decompression tables IV: Extension to Air and N_2-O_2 saturation diving, in: U.S. Navy (Ed.), 1986.

[15] Y.J. Parsons, P.K. Weathersby, S.S. Survanshi, E.T. Flynn, Statistically Based Decompression Tables V: Haldane-Vann Models for Air Diving, in: U.S. Navy (Ed.), 1989.

[16] G.W. Albin, P.K. Weathersby, Statistically Based Decompression Tables VI: Repeat Dives on Oxygen/ Nitrogen Mixes, in: U.S. Navy (Ed.)Bethesda, MD, 1991.

[17] P.K. Weathersby, S.S. Survanshi, R.Y. Nishi, E.D. Thalmann, Statistically Based Decompression Tables VII: Selection and Treatment of Primary Air and N_2O_2 Data, in: U.S. Navy (Ed.), 1992.

[18] E.C. Parker, S.S. Survanshi, P.K. Weathersby, E.D. Thalmann, Statistically Based Decompression Tables VIII: Linear-Exponential Kinetics, in: U.S. Navy (Ed.)Bethesda, MD, 1992.

[19] E.C. Parker, S.S. Survanshi, E.D. Thalmann, P.K. Weathersby, Statistically Based Decompression Tables IX: Probabilistic Models of the Role of Oxygen in Human Decompression Sickness, in: U.S. Navy (Ed.)Bethesda, MD, 1996.

[20] S.S. Survanshi, P.K. Weathersby, E.D. Thalmann, Statistically Based Decompression Tables X: Real-Time Decompression Algorithm Using a Probabilistic Model, in: U.S. Navy (Ed.)Bethesda, MD, 1996.

[21] E.D. Thalmann, P.C. Kelleher, S.S. Survanshi, E.C. Parker, P.K. Weathersby, Statistically Based Decompression Tables XI: Manned Validation of the LE Probabilistic Model for Air and Nitrogen-Oxygen Diving, in: U.S. Navy (Ed.)Bethesda, MD, 1999.

[22] S. S.S., E.C. Parker, E.D. Thalmann, W. P.K., Statistically Based Decompression Tables XII: Volume I. Repetitive Decompression Tables for Air and Constant 0.7 ATA PO_2 in N_2 using a Probabilistic Model, in: U.S. Navy (Ed.)Bethesda, MD, 1997.
[23] S. S.S., E.C. Parker, E.D. Thalmann, W. P.K., Statistically Based Decompression Tables XII: Volume II. Repetitive Dive Tables: Air, in: U.S. Navy (Ed.)Bethesda, MD, 1997.
[24] S. S.S., E.C. Parker, E.D. Thalmann, W. P.K., Statistically Based Decompression Tables XII: Volume III. Exceptional Exposure Tables: Air, in: U.S. Navy (Ed.)Bethesda, MD, 1997.
[25] S. S.S., E.C. Parker, E.D. Thalmann, W. P.K., Statistically Based Decompression Tables XII: Volume IV. Repetative Dive Tables: 0.7 ATA PO_2 in N_2, in: U.S. Navy (Ed.)Bethesda, MD, 1997.
[26] S. S.S., E.C. Parker, E.D. Thalmann, W. P.K., Statistically Based Decompression Tables XII: Volume V. Exceptional Exposure Tables: 0.7 ATA PO_2 in N_2, in: U.S. Navy (Ed.)Bethesda, MD, 1997.
[27] H.D. Van Liew, E.T. Flynn, Graphical analysis: Decompression tables and dive-outcome data, in: U.S. Navy (Ed.)Panama City, FL, 2004.
[28] H.D. Van Liew, E.T. Flynn, Decompression tables and dive-outcome data: graphical analysis, Undersea & Hyperbaric Medicine, 32 (2005) 187-198.
[29] H.L. Andersen, Decompression sickness during construction of the Great Belt Tunnel, Denmark, Undersea & Hyperbaric Medicine, 29 (2002) 172-188.
[30] D.J. Doolette, Haldane Still Rules!, in: M.A. Lang, A.O. Brubakk (Eds.) Future of Diving:100 Years of Haldane and Beyond, Smithsonian Institution Scholarly Press2009, pp. 29-32.
[31] P.K. Weathersby, E.E.P. Barnard, L.D. Homer, K.G. Mendenhall, Stochastic description of inert gas exchange, Journal of Applied Physiology, 47 (1979) 1263-1269.
[32] P.K. Weathersby, K.G. Mendenhall, E.E.P. Barnard, L.D. Homer, S. Survanshi, F. Vieras, Distribution of xenon gas exchange rates in dogs, Journal of Applied Physiology, 50 (1981) 1325-1336.
[33] J.A. Novotny, D.L. Mayers, Y.F. Parsons, S.S. Survanshi, P.K. Weathersby, L.D. Homer, Xenon kinetics in muscle are not explained by a model of parallel perfusion-limited compartments, Journal of Applied Physiology, 68 (1990) 876-890.
[34] D.J. Doolette, R.N. Upton, C. Grant, Diffusion-limited, but not perfusion-limited, compartmental models describe cerebral nitrous oxide kinetics at high and low cerebral blood flows, Journal of pharmacokinetics and biopharmaceutics, 26 (1998) 649-672.
[35] D.J. Doolette, R.N. Upton, C. Grant, Countercurrent compartmental models describe hind limb skeletal muscle helium kinetics at resting and low blood flows in sheep, Acta physiologica Scandinavica, 185 (2005) 109-121.
[36] D.J. Doolette, R.N. Upton, D. Zheng, Diffusion-limited tissue equilibration and arteriovenous diffusion shunt describe skeletal muscle nitrous oxide kinetics at high and low blood flows in sheep, Acta physiologica Scandinavica, 172 (2001) 167-177.
[37] D.J. Doolette, R.N. Upton, C. Grant, Altering blood flow does not reveal differences between nirtogen and helium in brain or in skeletal miracle in sheep, Journal of Applied Physiology, 119 (2015) 586-594.
[38] D.J. Doolette, R.N. Upton, C. Grant, Altering blood flow does not reveal differences between nitrogen and helium kinetics in brain or in skeletal miracle in sheep, Journal of Applied Physiology, 118 (2015) 586-594.
[39] R.Y. Nishi, G.R. Lauckner, Development of the DCIEM 1983 decompression model for compressed air diving, in: Department of National Defence - Canada (Ed.), Defence and Civil Institute of Environmental Medicine, Downsview, Ontario, Canada, 1984.
[40] S. Goldman, A new class of biophysical models for predicting the probability of decompression sickness in scuba diving, Journal of Applied Physiology, 103 (2007) 484-493.

[41] F.G. Murphy, E.A. Hada, D.J. Doolette, L.E. Howle, Probabilistic pharmacokinetic models of decompression sickness in humans, Part 1: Coupled perfusion-limited compartments, Computers in Biology and Medicine, 86 (2017) 55-64.
[42] F.G. Murphy, E.A. Hada, D.J. Doolette, L.E. Howle, Probabilistic pharmacokinetic models of decompression sickness in humans, Part 2: Coupled perfusion-diffusion models, Submitted, (2017).
[43] C. Balestra, P. Germonpre, Correlation between Patent Foramen Ovale, Cerebral "Lesions" and Neuropsychometric Testing in Experienced Sports Divers: Does Diving Damage the Brain?, Front Psychol, 7 (2016).
[44] D. Cialoni, M. Pieri, C. Balestra, A. Marroni, Flying after diving: should recommendations be reviewed? In-flight echocardiographic study in bubble-prone and bubble-resistant divers, Diving Hyperb Med, 45 (2015) 10-15.
[45] P. Germonpre, C. Balestra, Preconditioning to reduce decompression stress in scuba divers, Aerospace Medicine and Human Performance, 88 (2017) 114-120.
[46] P. Germonpre, J.M. Pontier, E. Gempp, J.E. Blatteau, S. Deneweth, P. Lafere, A. Marroni, C. Balestra, Pre-dive vibration effect on bubble formation after a 30-m dive requiring a decompression stop, Aviation Space and Environmental Medicine, 80 (2009) 1044-1048.
[47] K. Lambrechts, C. Balestra, M. Theron, A. Henckes, H. Galinat, F. Mignant, M. Belhomme, J.-M. Pontier, Venous gas emboli are involved in post-dive macro, but not microvascular dysfunction, European Journal of Applied Physiology, 117 (2017) 335-344.
[48] S.R. Thom, M. Bennett, N.D. Banham, W. Chin, D.F. Blake, A. Rosen, N.W. Pollock, D. Madden, O. Barak, A. Marroni, C. Balestra, P. Germonpre, M. Pieri, D. Cialoni, P.N.J. Le, C. Logue, D. Lambert, K.R. Hardy, D. Sward, M. Yang, V.B. Bhopale, Z. Dujic, Association of microparticles and neutrophil activation with decompression sickness, Journal of Applied Physiology, 119 (2015) 427-434.
[49] R.A. Horn, C.R. Johnson, Matrix analysis, [Reprinted with corr.] ed., Cambridge University Press, Cambridge Cambridgeshire ; New York, 1991.
[50] M.F. Morales, R.E. Smith, On the theory of blood-tissue exchange of inert gases: VI. Validity of approximate uptake expressions, Bulletin of Mathematical Biophysics, 10 (1948) 191-200.
[51] S.S. Kety, The Theory and Applications of the Exchange of Inert Gas at the Lungs and Tissues, Pharmacological Reviews, 3 (1951) 1-41.
[52] E.D. Thalmann, E.C. Parker, S.S. Survanshi, P.K. Weathersby, Improved probabilistic decompression model risk predictions using linear-exponential kinetics, Undersea & Hyperbaric Medicine, 24 (1997) 255-274.
[53] M. Abramowitz, I.A. Stegun, Handbook of mathematical functions, with formulas, graphs, and mathematical tables, Dover Publications, New York, 1972.
[54] S.B. Russ, A translation of Bolzano's paper on the intermediate value theorem, Historia Mathematica, 7 (1980) 156-185.
[55] R.P. Brent, An algorithm with guaranteed convergence for finding a aero of a function, The Computer Journal, 14 (1971) 422-425.
[56] K.A. Brownlee, Statistical theory and methodology in science and engineering, Wiley, New York,, 1960.
[57] P. Tikuisis, R.Y. Nishi, P.K. Weathersby, Use of the Maximum-Likelihood Method in the Analysis of Chamber Air Dives, Undersea Biomedical Research, 15 (1988) 301-313.
[58] L.E. Howle, P.W. Weber, R.D. Vann, M.C. Campbell, Marginal DCS events: their relation to decompression and use in DCS models, Journal of Applied Physiology, 107 (2009) 1539-1547.
[59] F.G. Murphy, A.J. Swingler, W.A. Gerth, L.E. Howle, Iso-risk air no decompression limits after scoring marginal decompression sickness cases as non-events, Submitted, (2017).
[60] R. Fletcher, Practical methods of optimization, 2nd ed., Wiley, Chichester ; New York, 1987.
[61] C.T. Kelley, Iterative methods for optimization, SIAM, Philadelphia, 1999.

690 [62] J.A. Nelder, R. Mead, A simplex method for function minimization, The Computer Journal, 7 (1965)
691 308-313.
692 [63] L.E. Howle, P.W. Weber, J. Nichols, Bayesian approach to decompression sickness model parameter
693 estimation, Computers in Biology and Medicine, 83 (2017) 3-11.
694 [64] D.J. Temple, R. Ball, P.K. Weathersby, E.C. Parker, S.S. Survanshi, The Dive Profiles and
695 Manifestations of Decompression Sickness Cases After Air and Nitrogen-Oxygen Dives. Volume I: Data
696 Set Summaries, Manifestation Descriptions, and Key Files, in: U.S. Navy (Ed.)Bethesda, MD, 1999.
697 [65] D.J. Temple, P.K. Ball, W. P.K., E.C. Parker, S. S.S., The Dive Profiles and Manifestations of
698 Decompression Sickness Cases After Air and Nitrogen-Oxygen Dives. Volume II: Complete Profiles and
699 Graphic Representations for DCS Events, in: U.S. Navy (Ed.)Bethesda, MD, 1999.
700 [66] L.E. Howle, Analytic gain in probabilistic decompression sickness models, Computers in Biology and
701 Medicine, 43 (2013) 1738-1747.
702 [67] G. Casella, R.L. Berger, Statistical inference, Brooks/Cole Pub. Co., Pacific Grove, Calif., 1990.
703
704

Table 1 Fitted values of the model parameters, eigenvalues, eigenvector matrix components, tissue gains, thresholds, and log likelihood function and predicted DCS cases for the five models investigated: Exponential-Exponential (EE1), Upper Triangular (UT), SKew-symmetric (SK), SYmmetric (SY) and GeNeral (GN). 95% confidence intervals are reported in superscript and subscript as increments with respect to the optimal value.

Parameters	EE1	UT	SK	SY	GN
$\lambda_1\left[\mathrm{min}^{-1}\right]$	$-0.424^{+0.078}_{-0.084}$	$-0.917^{+0.306}_{-0.467}$	$-0.320^{+0.032}_{-0.042}$	$-0.317^{+0.056}_{-0.087}$	$-0.317^{+0.052}_{-0.084}$
$\lambda_2\cdot 10\left[\mathrm{min}^{-1}\right]$	$-0.214^{+0.032}_{-0.043}$	$-0.084^{+0.009}_{-0.006}$	$-0.135^{+0.008}_{-0.002}$	$-0.167^{+0.017}_{-0.011}$	$-0.167^{+0.013}_{-0.010}$
$\lambda_3\cdot 10^2\left[\mathrm{min}^{-1}\right]$	$-0.217^{+0.015}_{-0.013}$	$-0.221^{+0.011}_{-0.015}$	$-0.221^{+0.004}_{-0.007}$	$-0.229^{+0.013}_{-0.012}$	$-0.229^{+0.011}_{-0.011}$
S_{12}		$-0.066^{+0.010}_{-0.015}$	$-1.266^{+0.105}_{-0.034}$	$-0.397^{+0.001}_{-0.002}$	$-0.397^{+0.001}_{-0.001}$
S_{13}		$0.572^{+0.021}_{-0.028}$	$-1.099^{+0.007}_{-0.024}$	$0.953^{+0.002}_{-0.002}$	$0.953^{+0.001}_{-0.002}$
S_{21}					$-0.397^{+0.075}_{-0.067}$
S_{23}		$-2.899^{+0.245}_{-0.311}$	$-0.503^{+0.020}_{-0.042}$	$-0.413^{+0.001}_{-0.001}$	$-0.413^{+0.038}_{-0.036}$
S_{31}					$0.953^{+0.003}_{-0.002}$
S_{32}					$-0.413^{+0.001}_{-0.001}$
α_1	$0.219^{+0.223}_{-0.132}$	$0.024^{+0.012}_{-0.010}$	$3.540^{+3.009}_{-2.270}$	$0.960^{+1.068}_{-0.524}$	$1.070^{+0.948}_{-0.625}$
$\alpha_2\cdot 10^2$	$0.670^{+0.210}_{-0.180}$	$0.0652^{+0.013}_{-0.011}$	$0.182^{+0.077}_{-0.072}$	$0.186^{+0.049}_{-0.044}$	$0.192^{+0.048}_{-0.042}$
$\alpha_3\cdot 10^2$	$0.186^{+0.037}_{-0.035}$	$0.046^{+0.040}_{-0.035}$	$0.102^{+0.020}_{-0.019}$	$0.145^{+0.037}_{-0.003}$	$0.145^{+0.034}_{-0.030}$
$b_1\left[\mathrm{atm}\right]$	$1.427^{+0.162}_{-0.165}$	$-0.076^{+0.014}_{-0.009}$	$0.879^{+0.027}_{-0.008}$	$0.662^{+0.051}_{-0.022}$	$0.662^{+0.058}_{-0.018}$
$b_2\left[\mathrm{atm}\right]$	$0.370^{+0.049}_{-0.046}$	$0.435^{+0.099}_{-0.097}$	$0.040^{+0.099}_{-0.077}$	$0.383^{+0.084}_{-0.061}$	$0.395^{+0.079}_{-0.061}$
$b_3\cdot 10\left[\mathrm{atm}\right]$	$-0.519^{+0.149}_{-0.151}$	$-0.367^{+1.047}_{-0.473}$	$0.355^{+0.267}_{-0.271}$	$-0.606^{+0.192}_{-0.177}$	$-0.606^{+0.200}_{-0.170}$
LL	−705.82	−697.33	−701.15	−692.11	−691.99
Predicted DCS	201.4	200.3	201.1	201.3	201.5

711 **Table 2** Model comparison through the log-likelihood difference test. All four multi-exponential
712 models pass the likelihood difference test, when compared with EE1. We can reject the EE1
713 model, in favor of any of the models including inter-tissue perfusions for prediction of DCS on
714 the training set ($P<0.05$). Conversely, the extra degrees of freedom introduced by the GN model
715 are not justifiable at the 5% significance level, when the test is conducted against the SY model.

	2 LL difference	Extra Degrees of Freedom	95% Limit Value	95% Test Passed
UT/EE1	16.98	3	7.81	TRUE
SK/EE1	9.33	3	7.81	TRUE
SY/EE1	27.41	3	7.81	TRUE
GN/EE1	27.65	6	12.59	TRUE
GN/UT	10.67	3	7.81	TRUE
GN/SK	18.32	3	7.81	TRUE
GN/SY	0.24	3	7.81	FALSE

716

717 **Table 3** Number of DCS cases predicted by the four multi-exponential and the null models for
718 the calibration data set "BIG 292". The predicted number of DCS cases are provided for the
719 groups of dives and analytically for each file present in the calibration data. All models seem to
720 adequately fit the calibration data set.

	Dives	Observed DCS	EE1	UT	SK	SY	GN
Single Air							
EDU885A	483	30	25.2	28.0	23.8	28.4	28.5
DC4W	244	8.4	7.7	5.8	7.7	8.0	8.3
SUBX87	58	2	1.9	1.8	2.5	1.7	1.9
NMRNSW	91	5.5	7.1	4.4	5.6	5.4	5.4
NSM6HR	57	3.2	4.6	2.4	4.0	3.4	3.4
Total	933	49.1	46.5	42.4	43.5	47.0	47.5
Single Air Decompression							
PASA	72	5.2	2.1	3.4	2.6	2.2	2.2
Repetitive air							
EDU885AR	182	11	11.9	11.1	10.6	11.5	11.5
DC4WR	12	3	0.6	0.8	0.8	0.7	0.7
PARA	135	7.3	7.9	8.3	8.2	7.3	7.2
Total	329	21.3	20.4	20.1	19.6	19.5	19.4
Multi-Level Air							
PAMLA	236	14.2	17.7	14.1	17.0	16.5	16.4
Single non-air							
NMR8697	477	12.8	18.7	15.9	15.4	15.3	15.2
EDU885M	81	4	3.6	4.2	3.0	4.6	4.6
EDU885S	94	4	3.2	4.0	3.7	3.9	3.9
EDU1180S	120	10	6.2	7.9	6.9	9.0	9.1
Total	772	308	31.7	32.1	29.0	32.8	32.8
Repetitive non-air							
EDU184	239	11	10.4	10.4	13.4	10.9	10.8
Air Saturation							
ASATEDU	120	15.7	13.4	12.3	10.6	12.0	12.0
ASATNSM	132	20.1	21.0	32.2	28.9	24.2	24.3
ASATNMR	50	1	5.0	2.2	3.7	4.1	4.1
Total	302	36.8	39.4	46.7	43.3	40.3	40.3
Non-air Saturation							
ASATARE	165	21.3	20.3	20.1	18.4	17.5	17.4
Multi-Level SDV; PO2=0.7 Decompressions							
PAMLAOD	134	6	8.0	7.1	8.6	10.3	10.2
Multi-Level SDV; PO2=0.7 Transits							
PAMLAOS	140	5.3	4.9	3.8	5.8	4.4	4.3

721

Table 4 Evaluation of the extrapolation capabilities of the five models on a set of data not included in the calibration data set and comparison with the EE1 model. The Pearson's $\chi 2$ results show that the UT model outperforms the other interconnected compartment models and the null model on the extrapolation data set. The UT model performs especially well on O_2 surface decompression dives. The other multi-exponential models (SK, SY, and GN) generalize more poorly than the null model (EE1) to the extrapolation data. Additionally, the null model (EE1) is the best performer in the single air category.

	Dives	Observed DCS	EE1	UT	SK	SY	GN
Single Air							
DC4D	797	19.4	19.1	16.1	22.9	22.6	23.5
EDU849LT2	141	29.8	16.7	8.1	8.5	10.8	11.0
NMR97NOD	103	3.4	4.2	3.8	4.6	3.1	3.1
EDU545	94	18.7	7.5	7.2	6.6	7.6	7.7
EDU557	568	27	50.8	32.3	31.4	37.8	38.3
EDU1157	46	15.6	14.9	28.2	11.7	14.4	14.5
EDU1351NL	143	2.7	5.3	3.5	3.5	4.3	4.3
NMRNSW2	91	5.5	7.1	4.4	5.6	5.4	5.4
Total	1983	122.1	125.6	103.8	95.0	106.2	107.8
Pearson's χ^2			0.0951	3.2401	7.7241	2.3957	1.9012
Repetitive air							
DC4DR	142	1	4.1	6.5	5.6	4.7	4.7
EDU657Corrected	142	4	11.3	9.2	8.9	9.5	9.5
Total	284	5	15.4	15.6	14.4	14.2	14.2
Pearson's χ^2			7.0109	7.2430	6.1722	5.9404	5.9590
Repetitive/Multilevel Non-Air							
EDU1180R	128	2	13.4	12.5	13.6	17.5	17.5
Pearson's χ^2			9.6936	8.7888	9.9010	13.7167	13.7276
Air + O2 Decompression							
DC8AOW	46	3.1	0.1	0.7	0.7	0.5	0.5
DC8AOD	256	3.2	1.2	3.8	3.3	3.7	3.7
NMR94EOD	284	17.9	8.4	8.2	9.6	10.9	10.9
Total	586	24.2	9.7	12.7	13.6	15.1	15.1
Pearson's χ^2			21.602	10.403	8.3270	5.4575	5.4637
O2 Surface Decompression							
DC8ASUR	358	10.1	14.7	7.3	7.7	11.4	11.6
DCSUREP	69	1	1.8	1.0	1.7	1.2	1.2
NMROSUR90	45	1	1.8	1.1	1.4	1.2	1.2
EDU1351SD	1035	43.3	70.2	47.3	50.5	52.0	52.5
Total	1507	55.4	88.5	56.7	61.3	65.9	66.6
Pearson's χ^2			12.376	0.0293	0.5604	1.6639	1.8690
Surface Decompression							
DC8ASURW	46	5	3.7	1.9	2.0	2.9	3.0

DCSUREPW	69	1	0.4	0.2	0.4	0.3	0.3
EDU545SUR	197	28.2	15.1	15.8	14.4	15.4	15.5
NMRASUR90	64	0	5.0	4.9	4.2	4.2	4.2
Total	376	34.2	24.2	22.8	20.9	22.9	23.0
Pearson's χ^2			4.0954	5.7615	8.4771	5.6192	5.4830
Submarine Escape							
UPS290	299	4	29.5	11.3	65.8	38.3	41.8
Partial LL			22.014	4.7387	58.038	30.730	34.192
Total DCS		246.9	306.3	235.4	284.6	280.0	285.9
Pearson's χ^2			76.890	40.204	99.209	65.523	68.595

729

730 **Figure 1** Schematization of the EE1, Goldman's 3CG and GN models. Circles indicate tissue
731 compartments; if filled they directly contribute to risk, otherwise they are associated with no risk.
732 For Goldman's 3CG model and our GN model, we have only sketched the external connection
733 from and to the circulatory system, not to make the figure unnecessarily cumbersome; also
734 Goldman's models have fixed thresholds, as opposed to all the other models, for which
735 thresholds are optimized.

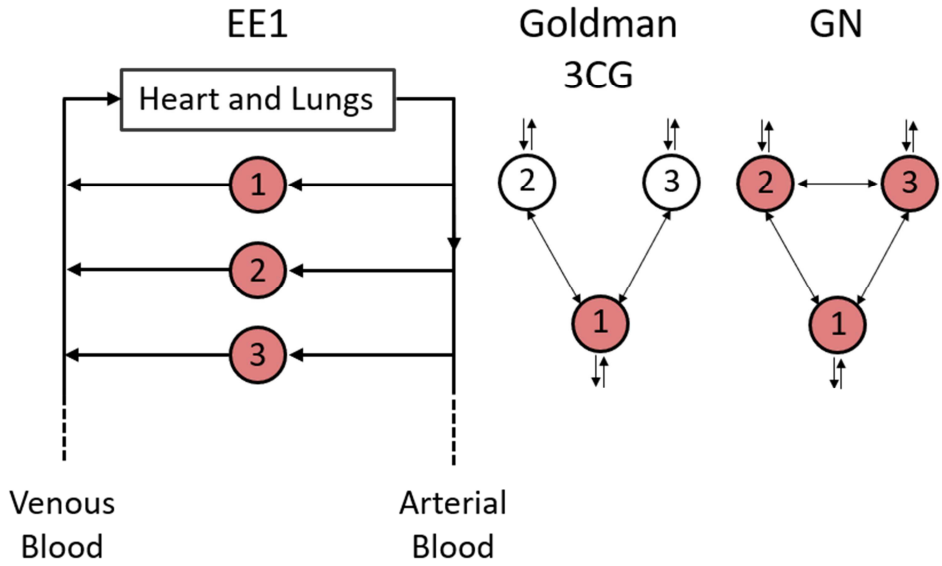

736
737
738
739
740

Figure 2 Schematization of the three-interconnected-compartment Upper Triangular (UT) model. Tissues are depicted with circles: the smaller the radius, the smaller the corresponding eigenvalue. Radii of the tissue times are not in scale. Black lines are of the order of unity, green lines are of the order of a tenth, blue lines are of the order of a hundredth. Tissues are ordered from most negative to least negative eigenvalues. For example, for the UT model, slower tissues are not directly affected by faster tissues: in fact, the slowest tissue (3) influences the tissue tension of the other tissues (1 and 2). Arrows directions are dictated by the sign of the term; so that $a_{ij} < 0$ implies an arrow going from tissue i to tissue j (since a_{ij} is relative to the influence of tissue j on i and the arrow shows that pressure of j diminishes for a positive increase on the pressure in tissue i).